Sounding Rocket Energy Management Using Cold-Gas Aerospike Thrusters: A Senior Capstone Design Course

Stephen A. Whitmore[1], Andrew R. Bath[2]

Abstract – *The design of a cold-gas energy management system for an amateur-class sounding rocket is presented. The design is an outcome of a required one-year senior design capstone course taught by the Mechanical and Aerospace Engineering Department at Utah State University. This course targets NASA's University Student Launch Initiative (USLI) competition organized and directed by Marshall Spaceflight Center. The design features a solid propellant primary rocket motor that provides a majority of launch impulse, and a secondary propulsion system that manages the energy level of the vehicle to reach a target apogee altitude. The secondary propulsion system was flown as the "engineering payload" for the USLI competition. The secondary system features a pulse-modulated cold gas bleed system with expansion ramps designed from aerospike nozzle theory. The energy management system was integrated with the airframe by placing the aerospike ramps around the primary solid motor case; this design added minimal aerodynamic drag to the configuration. Onboard navigation data are processed in a small onboard avionics computer to continuously estimate the total specific energy and potential altitude of the vehicle. When, required the onboard avionics activate the system to boost the energy level of the vehicle. Ground and flight test results are presented. Copyright © 2008 Praise Worthy Prize S.r.l. - All rights reserved.*

NOMENCLATURE		
A	=	state equation dynamics matrix
A_x	=	longitudinal acceleration, *g's*
A_y	=	lateral acceleration, *g's*
A_z	=	normal acceleration, *g's*
B	=	state equation input matrix
C	=	measurement equation matrix
C_D	=	drag coefficient
C_{D0}	=	incompressible drag coefficient
C_g	=	longitudinal center of gravity, *cm*
C_p	=	center of pressure, *cm*
E	=	total energy of the vehicle, *joules*
g	=	local acceleration of gravity, *m/sec²*
g_0	=	standard gravity, 9.8067 *m/sec²*
h	=	altitude, *m*
h_{apogee}	=	apogee altitude, *m*
$h_{perfectflite}$	=	PerfectFlite® altitude measurement, *m*
$h_{potential}$	=	potential altitude, *m*
h_{target}	=	target altitude, *1609.32 m*
I	=	identity matrix
k	=	discrete time index
K	=	Kalman gain matrix
m	=	vehicle mass, *kg*
p	=	roll rate, *deg/sec*
$P_{(ij)}$	=	Kalman filter state covariance matrix
q	=	pitch rate, *deg/sec*
Q	=	state noise covariance matrix
r	=	yaw rate or radial position, *deg/sec or cm*

R	=	measurement noise variance, *m²*
t	=	time, *s*
t_{apogee}	=	time to apogee, *s*
u	=	body-axis longitudinal velocity, *m/sec*
U	=	state equation input vector
u/V	=	normalized velocity defect
v	=	body axis lateral velocity, *m/sec*
V	=	velocity, *m/sec*
w	=	body axis normal velocity, *m/sec*
y	=	lateral position behind model, *cm*
z	=	vertical position behind model, *cm*
δ_{wake}	=	wake width, *cm*
Δt	=	sample interval, *sec*
ε	=	weighting function safety factor
γ	=	flight path angle, *deg.*
ϕ	=	roll angle, *deg*
Φ	=	state transition matrix
σ^2	=	noise covariance component
τ	=	Kalman filter time constant, *sec*
θ	=	pitch angle, *deg*
ζ	=	circumferential coordinate, *deg.*
$()_{k/k}$	=	Kalman filter update based on k measurements
$()_{k+1/k}$	=	Kalman filter prediction based on k measurements
$()_{k+1/k+1}$	=	Kalman filter update based on $k+1$ measurements

I. Introduction

The development of a unique two-semester capstone senior design course instructed by the Mechanical and Aerospace Engineering (MAE) and Electrical and Computer (ECE) Departments at Utah State University (USU) during the 2011-2012 academic hear is described herein. This case study presents the implementation of a successful capstone class that achieved all of its educational and technical objectives, and was selected as the winner of the 2011 NASA University Student Launch Initiative (USLI) competition. It is hoped that the materials presented in this paper will serve as a guide for other academic institutions wishing to undertake a similarly ambitious project. This project clearly demonstrates that when challenged and properly guided, undergraduate students can accomplish amazing things.

This design course was unique in that it specifically targeted the USLI launch competition organized and directed by the Marshall Spaceflight Center in Huntsville AL. The USLI competition tasks student teams to design and build a reusable rocket that can carry and safely recover working science or engineering payloads. The USLI competition judges the overall winners according to a scoring rubric that includes design reports and presentations, and a final written report describing the flight experiment results. A key element of the scoring rubric is the "altitude prize" for the team that comes closest to exactly 1-mile above the local ground level (AGL). The USLI concludes each spring with a daylong launch event near NASA's Marshall Space Flight Center. The NASA Office of Education, the Exploration Systems Mission Directorate (ESMD), and the NASA Space Grant Consortium in part sponsored this project. The course materials adhere to the standards of the Accreditation Board for Engineering and Technology (ABET), and are constructed to be relevant to key research areas identified by ESMD.

II. Capstone Design Course Overview

As described in the introductory section, the course material developed for this capstone class adheres to ABET-prescribed standards. ABET is recognized by the U.S. Government as the accreditation organization for higher-education programs in applied sciences, engineering, and technology. In the year 2000 ABET established a new program for accreditation review termed Engineering Criteria 2000" (EC2000), EC2000 changed the review perspective from qualitative evaluation to one based on program-defined missions, outcomes, and objectives. A major EC2000 requirement specifically states "Students must be prepared for engineering practice through a curriculum culminating in a major design experience based on the knowledge and skills acquired in earlier course work and incorporating appropriate engineering standards and multiple realistic constraints." As defined by ABET "Engineering design is the multi-disciplinary process of

devising a system, component, or process to meet desired needs. It is a decision-making process (often iterative), in which the basic sciences, mathematics, and the engineering sciences are applied to convert resources optimally to meet these stated needs." Here students are expected to engage in a culminating major design experience that requires cross-disciplinary efforts and a physical design realization.

Senior design capstone courses, when properly structured, provide students with a unique experience not generally available in an academic environment. Capstone courses involving multiple students require teamwork and application of industry-developed systems engineering processes that span the development cycle of the project. Students must make self-directed decisions to meet program objectives. Making these decisions properly requires significant use of problem solving, measurement, and experimental skills. Selecting a design concept that allows a small-scale prototype-demonstrator to be constructed within the academic-year time and budget constraints is a major challenge. A balance between "achievability" and "creativity" must be struck to achieve a realizable, successful design.

II.1. The USLI Competition as a Template for the Senior Design Capstone Experience

In industry, the client or customer provides much of the program structure including design requirements, budget, and program schedule. These constraints do not exist in an academic design class. Here the instructor must artificially prescribe the budget, design requirements, and schedule; and it is often difficult to get a high level of student interest in these artificially drafted requirements. With an excessively open-ended senior design course, students must be responsible for inventing client requirements, the design methodology, and then eventually constructing a design to meet their own requirements. This is an approach fraught with danger.

One of the major enemies of a successful program is "mission creep." Mission creep more often than not leads to a program stalling or collapsing under its own weight. Because of limited resources and student experience levels, undergraduate design projects are especially susceptible to mission creep. A "tried and true" way to keep a program on track is consistent adherence to a well-defined Design Reference Mission (DRM). A well-defined DRM allows top-level program requirements to be achieved, but limits the design scope and restricts unnecessary requirement growth. Targeting the USLI competition automatically produces a clearly defined DRM.

The USLI competition rules and scoring rubric items are used to set the top-level design requirements for the USU capstone design class. Thus the USLI becomes a natural customer for the class; and getting student "buy-in" is significantly easier. The top-level design schedule and milestones are pre-determined by the USLI competition rules. Students are required to develop and strictly adhere to a project schedule that conforms with

the prescribed USLI schedule. The top-level project objectives are very clear; fly safely and win the competition! The USU Entry into the Competition, officially named "Team Chimaera," was named after a mythical beast that was hybrid of many animal parts. This moniker certainly describes the final design that resulted.

III. Systems Engineering

The large size of the Chimaera team and the complex interdisciplinary nature of the design project required the use of formal systems engineering and management concepts throughout the class. As feasible these processes were modeled on well-documented, formal processes widely used within NASA, the Department of Defense (DoD), and the aerospace industry. Taking into account that seniors in college lack professional experience and background; as necessary, condensed subject matter lectures were incorporated into the class content. A few of the adapted systems engineering tools and procedures used in the design process will be discussed in eh following sub-sections.

III.1. Design Team Organization

The USLI-prescribed process closely emulates an industry-style design cycle. The USLI competition requires the students to submit a formal response to a NASA-issued Request for Proposal (RFP). The quality of the student team's response to the RFP determines whether or the team is for selected the USLI competition. Once selected, the team must submit to formal design reviews including a preliminary design review (PDR), a critical design review (CDR), and a flight readiness review (FRR). Both written and oral presentations are required. These reviews are major components of the overall USLI scoring rubric.

One of the most important aspects of a capstone design course is the presentation of condensed introductory materials that provide sufficient project background and technical information. This upfront material allows the students to begin making meaningful design contributions very early in the academic year. This early portion of the class also provides assessment metrics that allow students to be assigned to project aspects best suited to their skills and interests. This early evaluation period allows the discipline sub-teams to be optimally populated.

Discipline sub-teams were structured along traditional industry-style management lines. The team elected two undergraduate student members to serve as Chief Engineer and Systems Engineer. The Chimaera team consisted of 13 undergraduate students taking the class for credit and 4 graduate research/teaching assistants. When the faculty instructor was not available, graduate assistants assisted the undergraduate students in various technical discipline areas. The experiences and subject matter expertise provided by graduate assistants were essential for accomplishing the project goals and objectives.

III.2. Requirements Analysis

Table 1 presents the top-level design requirements. Vehicle design requirements come from three primary sources; 1) USLI competition-specified requirements, 2) compliance with safety codes, and 3) derived-secondary design requirements. The National Association of Rocketry (NAR)[i], and the National Fire Prevention Association (NFPA)[ii] specify the primary safety codes governing the rocket operation. This table lists the key requirements followed by the source. In the second column of this table the label USLI represents NASA competition rules, NAR represents National Association of Rocketry requirements and NFPA represent national USDA fire safety code driven requirements. The label USU represents level 2, project-derived requirements. Level 3 project requirements are too numerous to be listed in this table.

III.3. Concept of Operations

A key enabler a successful design is to development of a well-defined Concept of Operations (CONOPS). The CONOPS clearly defines operational concepts in a single figure, and allows an independent audience to understand the primary design and operation theory at a glance. The CONOPS allows subsystem design teams to scope the required levels of efforts very early in the program. Once established, the CONOPS should not be modified unless the program reaches a clear design or operational limit.

One of the "hard and fast" rules of the USLI competition is that launch teams must use a National Association of Rocketry (NAR) certified[iii] commercially available, hobby rocket motor for the main boost-element of the vehicle. Hobby rocket motors are not as well characterized as military or NASA-certified motors, and manufacturer specifications for total impulse among a particular type or class of motors can vary by as much as 20%. An impulse variability of 20% results in an apogee altitude error in excess of 300 meters. Consequently, the USU Chimaera team concluded that a closed-loop energy management system was required to "hit" the desired target-altitude at an accuracy level that is competitive to win the USLI competition.

Previous USU entries into the USLI competition solved this problem with a closed-loop energy management system that used air brakes to modulate the total energy of the rocket. The previous design philosophy was to "aim high and bleed energy" using four deployable and retractable airbrakes mounted near the rocket boat tail. The brakes were deployed at prescribed waypoints, and the energy management

---

[i] *"National Association of Rocketry Safety Information,"* http://www.nar.org/safety.html, [Retrieved 7 July 2011].
[ii] "National Fire Protection Association, Codes & Standards," http://www.nfpa.org, [Retrieved 7 July, 2011].
[iii] *"NAR Certified Motors,"* National Associate of Rocketry, http://www.nar.org/SanT/NARenglist.shtml, [Retrieved 4 December, 2010.]

system running on the onboard avionics computer determined the deployment times. The target total energy-state is approached asymptotically from above.

TABLE 1. TOP-LEVEL DESIGN REQUIREMENTS.

Statement of Key Requirement	Requirement Source
Rocket apogee shall not exceed 1706 meters above ground level	USLI
Rocket shall carry a scientific or engineering payload	USLI
Rocket shall be recoverable and reusable	USLI
Cost of all flight hardware shall not exceed $5000 USA dollars	USLI
Students shall perform all systems engineering and design	USLI
Students shall perform critical manufacturing and fabrication, professional machinists may be used but interface drawings shall be student prepared	USLI
Propulsion System Requirements • *Hot-gas propulsion elements shall use commercially available NAR or Tripoli certified high power or hybrid rocket motor*	USLI, NAR
•*Total cold-gas propulsion elements shall produce a total impulse less than 320N-simpulse*	NFPA 1112, 1127 Model Rocketry Codes
•*Cold-gas thrust elements shall produce less than 80 N thrust*	
The rocket shall approach within 16 meters (1%) of the target altitude of 1609.32 meters. •*Design shall target 95% confidence level with all error sources considered*	USU
All cold-gas augment system components shall fit within the main body tube of the vehicle with no external protuberances	USU
Rocket shall launch from rail with a minimum velocity of 15 m/s	USY
Structural members shall have an ultimate design load factor of safety of • *2.5 when component is designed by analysis only* •*1.25 when component has been proof loaded*	USU
Rocket will measure in-flight aerospike ramp surface pressures	USU

Because of newly established launch-range safety restrictions, the USLI scoring rubric for the altitude prize has been significantly modified to severely penalize teams that exceed the one-mile altitude limit. Furthermore, any rocket exceeding the target altitude by more than 100 meters will be disqualified from the competition. Thus the previous "aim high" strategy is far too risky with regard to the competition rules, and has been being replaced by an "aim low and boost energy" strategy.

Figure 1 shows the revised CONOPS for this vehicle. The airbrakes are replaced with small aerospike-based thrusters, and energy is added instead of depleted. The design uses an L-class solid rocket motor to boost the launch vehicle to a projected altitude 50-150 meters below the one-mile target. Following the main motor burnout, two small cold-gas aerospike thrusters are operated to augment the vehicle energy level. A closed-loop algorithm calculates and manages the vehicle energy by pulsing the cold-gas thrusters. The dashed lines of the CONOPS figure represent augmentation pulses that trim the vehicle energy level. Multiple pulses can occur; the energy management feed

back algorithm calculates the specific number of pulses that are required. A detailed description of the C-BAS system hardware is presented in *Payload Overview* and *Avionics* sub-sections of this report. A detailed description of the vehicle energy management algorithm is presented in *Energy Management* section of this report.
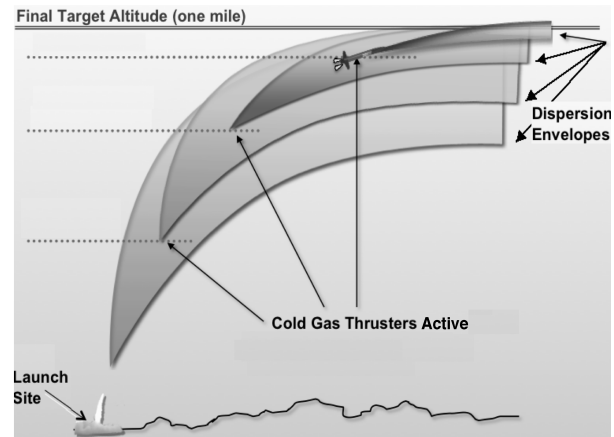

FIGURE 1. CONCEPT OF OPERATIONS.

This CONOPS allows the target altitude to be approached asymptotically from below, and minimizes the risk of overshooting the cap-altitude (1706 meters) for the USLI competition. The official project designation for the cold-gas base-area bleed augmentation system is the acronym C-BAS. For the remainder of this paper the C-BAS designation will be used to indicate a reference to the energy management system whole or component parts.

Figure 2 shows flight simulation results comparing a typical un-augment ballistic trajectory against a trajectory with C-BAS energy management active. The un-augmented ballistic trajectory reaches an apogee of approximately 1500 meters above the launch ground level. In the augmented trajectory as soon as the vehicle drag, predicted by the axial deceleration level, drops below the nominal C-BAS thrust-level the C-BAS system is activated. Based up on the best knowledge of the vehicle performance parameters, flight simulations predict that the nominal C-BAS activation event occurs at an altitude of approximately 1000 meters above the ground level and 8 seconds into the flight.

Once activated the C-BAS operates continuously to compensate for any defect in the post-burnout energy level. Once the vehicle energy reaches the desired level, the C-BAS system is pulsed to negate the effects of drag and "trims" the desired flight energy level. The USLI rules specifically prohibit forward thrusting devices, thus no mechanism for attenuating energy in the event that the rocket has excessive energy was available with the C-BAS system.
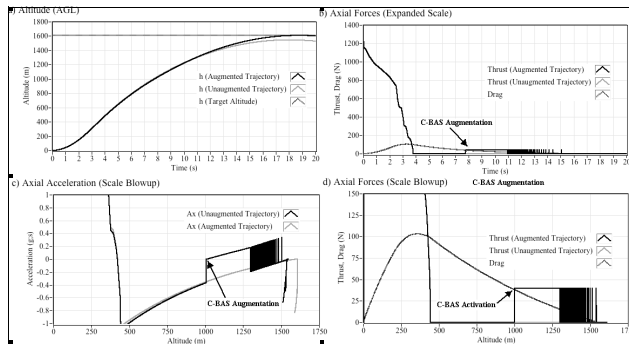
FIGURE 2. COMPARISON OF AUGMENTED AND BALLISTIC FLIGHT TRAJECTORIES.

IV.   Final Vehicle Design

This section presents only the final design for the vehicle, dubbed "the Javelin" by the Chimaera team. The design evolution and details regarding the subsystem verification testing used to characterize the component performances can be found in the student design review documents submitted to NASA.[iv] Key ground and flight test results will be presented later *Results and Discussion* section of this paper. Detailed descriptions of the test facilities and instrumentation will not be presented.

IV.1.   Vehicle Overview

The Javelin has a total launch mass of 12.59 kg, and has a tip-to-tail length of 225 cm. The aft section of the rocket houses the Cesaroni L730 solid propellant motor and C-BAS payload. Both the solid motor and C-BAS were tested extensively to verify that available impulse levels are sufficient to meet mission objectives.

The Javelin launches on a student-built mobile system featuring a 4.5-meter aluminum truss-launch rail. This mobile system serves as a transport trailer for the rocket and support equipment and acts as a base for the launch platform. The launch rail is an integral part of the trailer used to transport the Javelin. Adjustable jacks on the mobile launch platform allow the orientation of the launch rail to be adjusted to the desired condition.

The rocket body was constructed from Blue Tube 2.0®.[v] Blue Tube is an extremely lightweight and durable vulcanized-rubber reinforced phenolic material designed for amateur rocketry use. The vehicle was stabilized using three fixed tapered-rectangular fins constructed from a honeycomb fiberglass composite.

The recovery system features a dual redundant deployment system using nylon parachutes with Kevlar harnesses sized to keep the descent rate within ranges mandated by USLI competition rules. The drogue parachute is 76 cm in diameter and the main parachute is 305 cm in diameter. Two pressure altimeters are used

for dual-redundant deployment of the recovery system's parachutes. One of the altimeters was also designated to provide the official altitude measurement for the USLI competition. The avionics suite will be discussed in detail in later in this section of the document of this design document.

IV.2.   Motor Selection

Table 2 lists the properties of the down-selected Cesaroni L-730[vi] solid rocket motor. The Cesaroni is classified by NAR as an L-impulse class rocket, and is reusable. The external motor case is constructed of aluminum, with a phenolic insulating sleeve. The reloadable fuel grain consists of 6 "Bates" fuel grain segments with each segment approximately 10 cm in length. Total propellant for each reload is 1.351 *kg*, and the loaded motor mass is 2.247 *kg*. The accompanying phenolic nozzle is designed for a single use. The nozzle has a conical design, the nominal throat area is 1.90 *cm²*, and the nominal expansion ratio is 3.25.

Two options were investigated for the cold-gas augmentation system, carbon dioxide (CO_2), and high-pressure air (HPA). Even though HPA has a higher I_{sp} than CO_2, the higher HPA component weights resulted in unsatisfactory propellant mass fractions and volumes, and in the end carbon dioxide was selected as the working fluid. Mandating that the nominal thrust of the C-BAS exceeds the drag of the vehicle before operation insures that the fluid leaving the tank exit is liquid. Insuring a liquid tank exit state minimizes thrust variability and tank pressure drop due cooling as vapor state fluid exist the tank. Details of the cold-gas augmentation system (C-BAS) will be presented in the *Final Design* section of this report.

TABLE 2. CESARONI L-730 SOLID ROCKET MOTOR PROPERTIES.

Motor case Diameter / Length	*54mm / 64.9 cm*
Average Thrust / Burn Time	*730 N / 3.8 s*
Total Impulse / Effective Specific Impulse	*2765 N-s/ 209 s*
Nozzle Throat Area / Expansion ratio	*1.90 cm² / 3.25*
Cost per Reload	*$160*

IV.3.   Payload Overview

As described previously in the Systems Engineering section, the primary vehicle payload is a cold-gas energy management system whose external contour is derived from aerospike nozzle theory. The aerospike-derived isentropic expansion ramps are wrapped around the primary solid motor core. This concentric thruster design fits entirely within the main rocket body tube, and when compared to "strap-on" thrusters, adds negligible aerodynamic drag to the external configuration. Figure 3 shows the integration of the cold-gas thruster ramps thrusters into the rocket base area.

[iv] "Chimaera Advanced Student Built Rocketry, User documentation, http://Chimaera.usu.edu/projects/usli/documents, [Retrieved 7 July 2010].

[v] "Blue Tubes," http://www.apogeerockets.com/blue_tubes.asp, [Retrieved 11 July 2011].

[vi] "Motor Performance Data Online," http://www.thrustcurve.org, [Retrieved 7 July 2011].

The external expansion ramp contour was designed to allow an isentropic expansion from the operating plenum pressure to external ambient pressure conditions. The method developed by Lee and Thompson,[1] was used to design the spike contour. Each spike had an expansion ramp width of 1.5 cm, a length of 4.4 cm, and a throat exit area of approximately 0.072 cm2. The entire thruster was approximately 6.6 cm in length. Side fences were used to limit the lateral expansion of the plume and the resulting thrust loss.[2] The ramps were truncated at 85% of their theoretical length. When operated at 850 kPa (120 psig) plenum pressure the combined system was designed to produce a nominal thrust that varies between approximately 10-15 Newtons.

The C-BAS pneumatic components consist of a CO_2 tank, pressure regulator, solenoid valve, steel-mesh propellant tubing, and aerospike thrusters. The in-line regulator has an output pressure that is variable from 450 psig (3200 kPa) to 80 psig (640 kPa). This regulator drops the flow from saturation pressure in the tank, approximately 5000 kPa, to the design operating pressure, approximately 1250 kPa. Standard paintball-class tanks carry the onboard CO_2 in a saturated-liquid form. Interchangeable options for both 24 oz (0.68 1 kg) and 12 oz (0.34 kg) CO_2 tank sizes are provided for in the design.
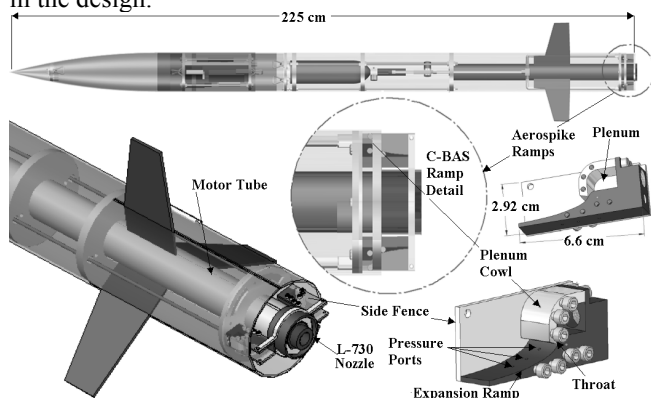

FIGURE 3. INTEGRATION OF AEROSPIKE THRUSTERS INTO VEHICLE BASE AREA.

IV.4. Avionics

A suite of onboard instruments was carried to measure the vehicle trajectory and manage the flight systems. Figure 4 shows the primary avionics systems components. The main onboard navigation instrument is miniature inertial measurement unit (IMU) built by Micro-Strain®, Inc.[vii] The IMU features a high-performance miniature attitude heading reference system that includes embedded tri-axial accelerometers, rate-gyros, magnetometers, and a temperature sensor.

The IMU data are complemented by ground-referenced altitude measurements from a pressure based PerfectFlite® Altimeter.[viii] Additional flight instruments

include 6 C-BAS expansion ramp surface pressure transducers. The pressure ports are located on each ramp 1, 2, and 3 cm aft of the C-BAS thruster throat exit. A separate inexpensive R-DAS[ix] (Rocket data Acquisition System) system was flown to log the ramp pressures. The R-DAS system is separate from the main avionics.

Navigation data are processed in a small onboard avionics computer using a Kalman-filter to continuously estimate the total specific energy and potential altitude of the vehicle. The IMU sensor data is blended in an internal microprocessor running a sensor fusion algorithm to provide inertial navigation quality output parameters. User-selectable output parameters include Euler angles, rotation matrix components, velocity vector components, acceleration vector components, 3-axis angular rates, and 3-axis magnetic field components.

Onboard control law calculations, data flow management, and C-BAS activation are controlled using a GumStix® Overo-Tide micro-computer.[x] The GumStix is a 17 mm x 58 mm, 600 MHz single-board computer that features the open-source Overo development platform. A Ubiquiti® Bullet[xi] 2HP WiFi transceiver provides communications between the onboard flight computer and a ground based laptop receiving station. The "Bullet" transmits using an industry standard *IEEE 802.11 G* wireless telemetry link. A user datagram protocol (UDP) was used to packet the streaming downlink data. Options for a communications uplink were available but never implemented for this project.

The ground-based laptop runs an interface program, written in the National Instruments Labview 2010® programming language[xii] that allows direct control of all onboard functions including built-in test diagnostics, startup, and navigation algorithm startup settings. Finally this program receives and logs pertinent flight data including the cold-gas measurement parameters, IMU outputs, and system health bits.

IV.5. Recovery System

As mentioned in the introduction to this section, the vehicle featured a dual-deployment (drogue/main) and dual-redundant recovery system. Two PerfectFlite altimeters were used to initiate deployment. The primary PerfectFlite sensor was also used to as a part of the avionics navigation suite and provided the "official" attitude measurement for the USLI competition. When either altimeter senses apogee, a signal is sent fire electronic matches, which in turn fire dual redundant black powder ejection charges. Gases generated by the

[vii] 3DM-GX3TM-25, "Miniature Attitude heading Reference System, Technical Product Overview," MicroSAtrain, Inc. http://www.microstrain.com, [retrieved 12 July 2011].
[viii] "MiniAlt/WDTM User's Manual," PerfectFlite, Inc., www.perfectflite.com, [retrieved 1 June 2011].

[ix] R-DAS", AED electronics, http://www.aedelectronics.nl/rdas/links.htm, [retrieved 14 July 2011].
[x] "Gumstix, Dream, Design, Deliver," http://www.gumstix.com, [Retrieved 10 April 2010].
[xi] "Bullet, Revolutionary Outdoor Radio Device," http://ubnt.com/bullet, [Retrieved 12 July 2011].
[xii] "NI Labview," National Instruments, http://www.ni.com/labview, [Retrieved 8 June 2011].

black powder ejection charges separate the avionics bay from the main airframe and deploy the drogue parachute. To reduce drift, but slow the rocket enough for a safe landing, the main parachute is deployed at approximately 1000 ft (300 m) AGL. Table 3 lists the recovery system design operating parameters.
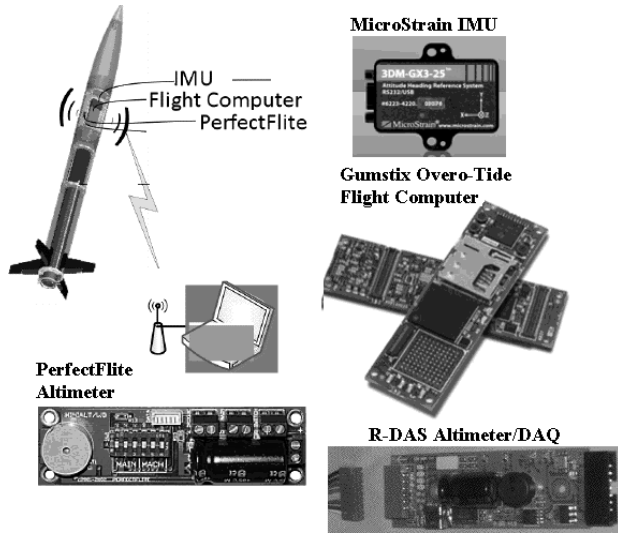

FIGURE 4. AVIONICS SYSTEM COMPONENTS.

TABLE 3. RECOVERY SYSTEM DESIGN AND OPERATING PARAMETERS.

Parameter	Drogue Parachute	Main Parachute
Parachute Type	Conical	Conical
Deployment Altitude (*m AGL*)	5032	300
Deployment Air Density (*kg/m³*)	1.031	1.163
Deployment Velocity (*m/s*)	42.58	22.26
Nominal Terminal Velocity (*m/s*)	23.65	5.64
Drag Coefficient	0.8	0.8
Reference Area (*m²*)	58.85	884.96
Peak Opening Load (*N*)	583.77	526.38

V. Kalman Filter Navigation Equations

As mentioned in the introductory section, the IMU and altimeter data are used to calculate the vehicle trajectory parameters in real time, and these results are used to predict apogee based on the overall energy level of the vehicle. This section describes the vehicle dynamics and Kalman filtering equations used to estimate the vehicle trajectory in real time.

V.1. State Equations

This application uses the discrete form of the Kalman filter equations, with the state equations discretized via trapezoidal rule. The continuous-time state equation describing the translational dynamics of the vehicle[3] is

$$
\begin{bmatrix} \dot{u} \\ \dot{v} \\ \dot{w} \\ \dot{h} \end{bmatrix} = \begin{bmatrix} 0 & r & -q & 0 \\ -r & 0 & p & 0 \\ q & -p & 0 & 0 \\ \sin\theta & -\sin\phi\cos\theta & -\cos\phi\cos\theta & -\frac{1}{\tau} \end{bmatrix} \cdot \begin{bmatrix} u \\ v \\ w \\ h \end{bmatrix} + \begin{bmatrix} A_x \\ A_y \\ A_z \\ 0 \end{bmatrix} + g \cdot \begin{bmatrix} -\sin\theta \\ \sin\phi\cos\theta \\ \cos\phi\cos\theta \\ 0 \end{bmatrix}
$$

(1)

When Eq. (1) is discretized via trapezoidal rule where both the current and previous frame IMU data are used to approximate the derivatives, the result is

$$
x_{k+1/k} = x_{k/k} + \frac{\Delta t}{2}\left[\left(A_{k+1} \cdot \tilde{x}_{k+1} + (B \cdot u)_{k+1}\right) + \left(A_k \cdot x_k + (B \cdot u)_k\right)\right]
$$

(2)

The state equation is assumed contaminated by additive, gasssian-distributed white noise. This noise has a covariance represented by the matrix Q_{k+1}. A model for the state noise covariance will be developed later in this section.

V.2. Observation Equations

When the sensed acceleration measurements are integrated "open-loop", the velocity and subsequent altitude estimates will drift with time, and a stable altitude measurement is needed to minimize this drift. For this application to PerfectFlite® altitude measurement is used to stabilize the integration. The resulting observation equation is

$$
\begin{bmatrix} h_{PerfectFlite} \end{bmatrix} = \begin{bmatrix} 0 & 0 & 0 & 1 \end{bmatrix} \begin{bmatrix} u \\ v \\ w \\ h \end{bmatrix}
$$

(3)

where the [u v w h]T is the current state vector estimate. The measurement matrix C, has an invariant form

$$
C = \begin{bmatrix} 0 & 0 & 0 & 1 \end{bmatrix}.
$$

(4)

Since the order of the measurement vector is 1, the measurement noise variance R_{k+1}, is a scalar quantity. A model for the measurement noise variance will be developed later in this document.

V.3. State Covariance Propagation

A simple Explicit Euler discretization algorithm uses only the current IMU data for the covariance propagation. This approach allows the covariance update to be performed without requiring real time matrix inversion. The explicit Euler discretization the approximate state transition matrix is written as

$$\Phi_{k+1} = [I + A_k \cdot \Delta t] =$$

$$\begin{bmatrix} 1 & r \cdot \Delta t & -q \cdot \Delta t & 0 \\ -r \cdot \Delta t & 1 & p \cdot \Delta t & 0 \\ q \cdot \Delta t & -p \cdot \Delta t & 1 & 0 \\ -M_{13} \cdot \Delta t & -M_{23} \cdot \Delta t & -M_{33} \cdot \Delta t & 1 - \dfrac{\Delta t}{\tau} \end{bmatrix}_k \quad (5)$$

The state transition matrix is used to propagate the state covariance assuming additive state noise with covariance Q_{k+1}. The resulting state covariance prediction equations is

$$P_{k+1/k} = \Phi_{k+1} P_{k+1/k} \Phi_{k+1}^T + Q_{k+1} \quad (6)$$

V.4. Kalman Gain Matrix

The Standard form of the Kalman gain matrix is

$$K_{k+1} = P_{k+1/k} C^T \left[C P_{k+1/k} C^T + R_{k+1} \right]^{-1} \quad (7)$$

Substituting in for the actual "C" matrix from Eq. (4), expanding and collecting terms, the flight-implemented Kalman gain matrix becomes

$$K_{k+1} = \begin{bmatrix} \dfrac{P_{14}}{P_{44} + R_{k+1}} \\ \dfrac{P_{24}}{P_{44} + R_{k+1}} \\ \dfrac{P_{34}}{P_{44} + R_{k+1}} \\ \dfrac{P_{44}}{P_{44} + R_{k+1}} \end{bmatrix}_{k+1/k} \quad (8)$$

V.5. Kalman Update Equations

The standard form of the Kalman state update equation is

$$\hat{x}_{k+1/k+1} = \hat{x}_{k+1/k} + K_{k+1} \cdot \left[Z_{k+1} - C \cdot \hat{x}_{k+1/k} \right] \quad (9)$$

Substituting in for K_{k+1} and C gives the form for the flight state update equation

$$\begin{bmatrix} u \\ v \\ w \\ h \end{bmatrix}_{k+1/k+1} = \begin{bmatrix} u \\ v \\ w \\ h \end{bmatrix}_{k+1/k} +$$

$$+ \begin{bmatrix} \dfrac{P_{14}}{P_{44} + R_{k+1}} \\ \dfrac{P_{24}}{P_{44} + R_{k+1}} \\ \dfrac{P_{34}}{P_{44} + R_{k+1}} \\ \dfrac{P_{44}}{P_{44} + R_{k+1}} \end{bmatrix}_{k+1/k} \left(h_{PerfectFlite_{k+1}} - \hat{h}_{k+1/k} \right) \quad (10)$$

The standard form of the covariance update equation is

$$P_{k+1/k+1} = \left[I - K_{k+1} \cdot C \right] P_{k+1/k} \quad (16)$$

Substituting for K_{k+1} and C gives the flight-implemented form of the covariance update equation

$$P_{k+1/k+1} =$$

$$\begin{bmatrix} 1 & 0 & 0 & \dfrac{-P_{14}}{P_{44} + R_{k+1}} \\ 0 & 1 & 0 & \dfrac{-P_{24}}{P_{44} + R_{k+1}} \\ 0 & 0 & 1 & \dfrac{-P_{34}}{P_{44} + R_{k+1}} \\ 0 & 0 & 0 & 1 - \dfrac{P_{44}}{P_{44} + R_{k+1}} \end{bmatrix} P_{k+1/k} \quad (11)$$

V.6. State Noise Covariance Model

As described earlier the state (Q_{k+1}) and measurement error (R_{k+1}) covariance models are necessary to complete the filtering algorithm. The state equation covariance model is derived from errors in the input data from the IMU measurements. The dominant error in the state equation results from the noise in the accelerometer and pitch angle measurements. Altitude errors due to roll and yaw angle are negligible. Additionally, cross axis errors are assumed to be negligible and all off-diagonal covariance terms are set to zero. Along a ballistic trajectory the angle of attack is small and $u >> \{v, w\}$, thus the altitude rate error due to IMU attitude errors can be approximated by

$$\delta \dot{h} = V \cdot \cos\theta \cdot \delta\theta \quad (12)$$

The discrete variance is then approximated by

$$\sigma^2 h \approx \Delta t^2 \left(V \cdot \cos\theta \right)^2 \cdot \sigma^2_\theta = \Delta t^2 \cdot V_{horizontal}^2 \cdot \sigma^2_\theta \quad (13)$$

The resulting state noise covariance model is

$$Q_{k+1} = \left(\Delta t \cdot g_0 \right)^2 \times$$

$$\begin{bmatrix} \sigma^2_{A_x} & 0 & 0 & 0 \\ 0 & \sigma^2_{A_y} & 0 & 0 \\ 0 & 0 & \sigma^2_{A_z} & 0 \\ 0 & 0 & 0 & \left(\dfrac{V_{horizontal}}{g_0} \right)^2 \sigma^2_\theta \end{bmatrix} \quad (14)$$

The first three parameters along the matrix diagonal represent the variances due to the IMU accelerometer uncertainties (*g's*), and the final parameter on the diagonal models the altitude variance due to the IMU attitude errors. Table 4 summarizes the expected IMU (Ref. vii) accelerometer, pitch attitude, and altitude-rate parameter errors.

TABLE 4. SUMMARY OF EXPECTED IMU PARAMETER
ERRORS.

$V_{horizontal},$ m/sec	$\{\sigma_{Ax}, \sigma_{Ay}, \sigma_{Az}\}$ (g's)	σ_θ (deg,radial)	$\dfrac{V_{horizontal}}{g}\sigma_\theta$ (s)
0	± 0.10 g's	± 2 deg. (0.035 rad)	0.000 sec
10	-	-	0.036 sec
20	-	-	0.072 sec
30	-	-	0.107 sec
40	-	-	0.142 sec
50	-	-	0.178 sec

V.7. Measurement Noise Covariance Model

The measurement error covariance model is calculated directly from the expected uncertainty in the *PerfectFlite* altitude measurement. The stated accuracy of the altitude measurement is +0.25-5% of reading. (Ref. viii) This value equates to approximately $\pm$*4-8 meters* measurement uncertainty at apogee. Because the PerfectFlite reading is judged to be the "truth" metric for altitude in the competition, the variance will be linearly diminished with time so that the filter weights the sensor altitude reading more and more heavily as apogee is approached. Thus the potential altitude output used to control the vehicle's energy level will be strongly tied to the perfect flight altitude reading. The prescribed adaptive weighting function for the PerfectFlite measurement noise is

$$\sigma_{h_{PerfectFlite}} = \pm 0.005 \cdot \hat{h}_{k/k} \cdot \left(1 - \frac{\hat{h}_{k/k}}{h_{target}}\right) + \varepsilon \qquad (15)$$

In Eq. 15 h_{target} is the target altitude of 1609.32 meters, $h_{k/k}$ is the current altitude estimate of the Kalman filter, and parameter ε is a small positive magnitude factor that prevents the measurement noise covariance from becoming *exactly zero* -- an event that would cause stability problems with the Kalman filter covariance propagation. Figure 5 plots the time-of-fight profile of Eq. (6) along a nominal flight trajectory. The minimum weighting (inverse of the error function) occurs shortly after motor burnout (5 seconds) and approaches maximum value just prior to reaching apogee (19.5 seconds). The "ε" safety-factor was set to 0.1 meter for this calculation.
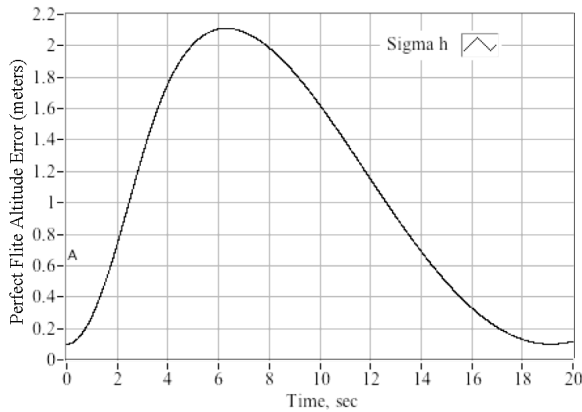

FIGURE 5. TIME-OF-FLIGHT PROFILE FOR MEASUREMENT NOISE WEIGHTING FUNCTION.

VI. Energy Management Algorithm

The energy management algorithm uses a balance of potential and kinetic energy to predict the vehicle apogee altitude based on Kalman filter estimates of 1/2 the squared velocity (*kinetic energy per unit mass*) and altitude (*potential energy per unit mass*). The feedback algorithm checks calculated potential altitude against a target reference. If the energy state of the vehicle is low, the algorithm commands the flight avionics to activate the energy management system by opening the CO_2 solenoid valve. When the energy state climbs to the prescribed value, the solenoid valve closes.

VI.1. Calculating the Potential Apogee Altitude

Key to the energy management described in the previous section is the "potential altitude" of the vehicle; derived from the sum of the gravitational potential energy and kinetic energy in the vertical direction. The potential altitude can be calculated using the body axis velocity and altitude estimates from the Kalman filtering algorithm. At any point along the trajectory the sum of the mass-specific potential energy is given by

$$\left(\frac{E}{m}\right)_{total} = g \cdot h + \frac{V^2}{2}. \qquad (16)$$

At any time following motor burnout the total energy state of the rocket at apogee can be calculated by

$$\left(\frac{E}{m}\right)_{apogee} = g \cdot h_{apogee} + \frac{V^2}{2} - \int_t^{t_{apogee}} \left(\frac{1}{2} \cdot \rho \cdot V^2\right) \cdot \left(\frac{C_D \cdot A_{ref}}{m}\right) \cdot V \cdot dt. \qquad (17)$$

The last term on the right hand side of Eq. (17) is the energy depleted by drag forces acting on the rocket. Eq. (17) can be rearranged to predict the apogee altitude based on the energy state (*potential + kinetic energy*) estimated at any point along the trajectory. Also, for ballistic trajectories with a nearly vertical initial launch angle, the horizontal velocity of the rocket at motor burnout remains nearly constant throughout the climb to altitude, and Eq. (17) reduces to

$$h_{apogee} = h_{(t)} + \frac{\left(V_{(t)} \cos\gamma_{(t)}\right)^2}{2 \cdot g} - \int_t^{t_{apogee}} \left(\frac{1}{2} \cdot \rho \cdot V^2\right) \cdot \left(\frac{C_D \cdot A_{ref}}{m \cdot g}\right) \cdot V \cdot dt. \qquad (18)$$

Near apogee the drag term in Eq. (19) diminishes, and the "near apogee" potential altitude calculation becomes

$$h_{potential} = h(t) + \frac{\left(V(t) \cdot \sin\gamma\right)^2}{2 \cdot g}. \qquad (19)$$

The available change in potential altitude equals the change in velocity resulting when a given mass of propellant is consumed.

VI.2. Target Altitude Scheduling

The drag loss term in Eq. (27) is path dependent and is difficult to accurately calculate in flight, especially with the C-BAS augmentation thrusters firing. The drag-loss parameter is best calculated pre-flight for a nominal trajectory and then used to schedule the "target altitude" as a function of the flight altitude. This approach allows the targeting algorithm to account for the anticipated drag-related energy loss along the flight path. The accumulated drag loss is added to the target altitude, nominally 1609.32 meters, to derive a target altitude schedule.

Figure 6 shows the potential altitude loss due to drag along the flight path, and compares the target altitude to the potential altitude calculated using Eq. (20). The true altitude is also plotted for comparison purposes. The plotted data are results for a representative trajectory using approximately 2/3rd's of the total available C-BAS impulse and the assumed mean C-BAS thrust level is 10 Newtons. Pre-scheduling the target altitude improves the algorithm efficiency and has the effect of requiring less toggling of the C-BAS impulse to achieve the desired altitude. Pre-scheduling the target altitude results a nominal 10% cold-gas propellant savings.
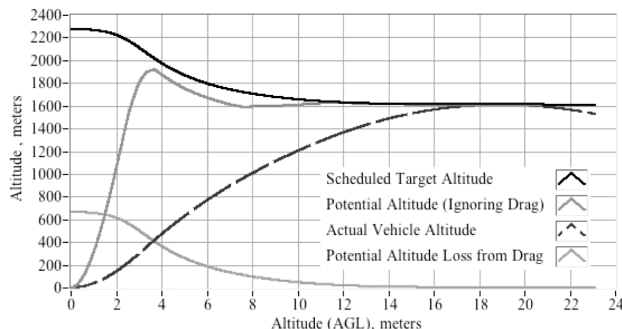
FIGURE 6. POTENTIAL ALTITUDE LOSS DUE TO DRAG AND TARGET ALTITUDE SCHEDULE.

VI.3. C-BAS Activation Control Law.

A simple pulse-width modulation algorithm is used to control the vehicle energy levels. Following the motor burn out, the onboard flight computer continually calculates potential altitude, axial deceleration, and drag of the vehicle. Due to the CO_2 being in a saturated state, there will be two-phase flow as the fluid exits the tank. Drawing vapor from the tank significantly cools the tank, and the gas pressure being delivered to the aerospike plenum chamber drops dramatically. Insuring that the thrust from the spikes exceeds the drag of the vehicle before operation insures that the fluid leaving the tank exit is liquid. Once the calculated drag drops below the predicted nominal C-BAS thrust level, the energy management algorithm is activated. Figure 7 shows the energy management calculation sequence. Here h_{min} is the altitude at which the drag drops below

the available thrust level, and h_{target} is the target apogee altitude.

VII. Ground Test and Evaluation

Extensive preliminary ground tests were performed to demonstrate the functionality of the flight subsystems and to calculate or measure key vehicle performance parameters. This section presents results of the ground evaluations performed to estimate and verify the vehicle aerodynamics, main launch motor performance, and C-BAS thruster performance characteristics.
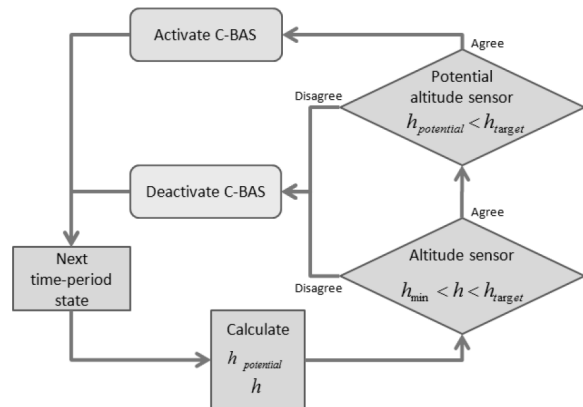

FIGURE 7. C-BAS ENERGY MANAGEMENT CONTROL LAW.

VII.1. Vehicle Aerodynamics

Since the Javelin is designed to fly passively along a ballistic trajectory, detailed knowledge of the vehicle longitudinal centers of pressure and center of gravity during flight was essential to insure both static and dynamic stability. Accurate knowledge of the drag coefficient was essential to insure proper operation of the energy management system.

Initial estimates of the vehicle lift, drag, and pitching moment coefficients were obtained using the Air Force missile flight dynamics code, Missile DATCOM.[4] The initial DATCOM drag coefficient estimates were corroborated using the commercial rocketry analysis code, AeroCFD,[xiii] and a skin-friction/pressure correlation model developed by Drew and Jen.[5] Finally, wind tunnel wake surveys were performed using a 1/5th scale model to directly measure the vehicle drag coefficient.

Static Stability

In the design phase, computer-aided design (CAD) models and mass-distribution spreadsheets were used to estimate the center of gravity (C_g) location. Once the vehicle was built these calculations were verified by direct measurements. Early center of pressure (C_p) estimates were derived using Barrowman's Method.[6] These C_p calculations were then verified using the Missile DATCOM, and AeroCFD. Finally, these results were experimentally verified through a series wind

---

[xiii] "AeroCFD® 7.0, Model Rocket CFD Program for Microsoft Windows By AeroRocket," http://www.aerorocket.com/aerocfd.html, [retrieved 12 July, 2011].

tunnel tests. The wind tunnel tests will be described later in this section. Figure 8 shows the calculated time-of-flight locations of C_g and C_p for the various computational models. The variation in static margin is also plotted.

A simple wind tunnel test was performed using a $1/5^{th}$ scale model of the Javelin to verify the analytical static-stability calculations. A rod was attached at the approximate center of gravity location allowing the model to pivot freely about that point. The attachment point was subsequently moved aft until the rocket no longer had a positive restoring moment. This neutral point was marked as the center of pressure. With the C_g behind the C_p, any disturbance caused the model to go unstable. Once the location of the center of pressure was determined, the rod was then moved back to actual scaled location of the Javelin's C_g. The model was placed at various trim angles and allowed to rotate freely. The stability was checked for predicted center of gravity locations at launch, motor burnout, and flight apogee. For angles less than 25 degrees the rocket returned and aligned with the airflow. Only minor overshoot was noted and the oscillation quickly damped. This result clearly indicates that the javelin airframe is both statically and dynamically stable for the ranges of C_g and C_p to be experienced in flight.

Wind Tunnel Wake Surveys

This section describes the experimental apparatus and procedures, and presents test results from wind tunnel wake surveys performed to measure the $1/5^{th}$ scale model drag coefficient. The Mechanical and Aerospace Engineering department at USU has at its disposal a small subsonic wind tunnel with an approximately *30 x 30 cm* wide by *100 cm* long test section. The empty wind tunnel can reach speeds of approximately 30 m/sec (*98 ft/sec*). This airspeed produces a dynamic pressure of approximately *0.48 kPa* (*10 lbf/ft²*).
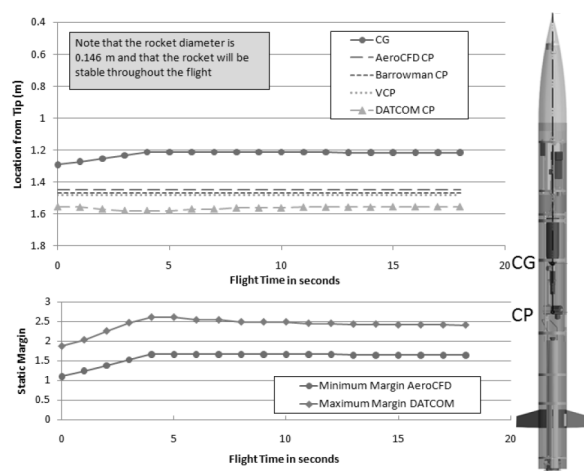

FIGURE 8. TIME-OF-FLIGHT CENTER OF MASS, CENTER OF PRESSURE, AND STATIC MARGIN PROFILES.

Because of the low dynamic pressure levels and small test section size, wake survey methods were

considered to be far more accurate for measuring the drag coefficient than direct load measurements using a support sting and force balance. Also, due to the potential for wall reflections and tunnel flow blockage at high angles of attack, only low angle of attack measurements are considered valid. Although the maximum tunnel speed is significantly lower than the maximum speeds reached by the rocket in flight; the wake survey methods nonetheless provide a good measure of the incompressible drag coefficient and results in a good "sanity check" on the analytical calculations.

For the wake surveys, the model was mounted on a moveable support rod, and a traversing pitot/static probe was mounted on a traversing rack and pinion drive. A small electrical motor drives the traversing mechanism, and the probe position is sensed by a small linear potentiometer. A high-resolution MKS® 223BD differential manometer sensed the differential pressure across the probe. Omegadyne® 142PC15A *0-15 psia* (*103 kPa*) absolute Omegadyne®143PC01D *±1 psid* (*±6.9 kpa*) differential pressure transducers sensed the tunnel reference total and static pressure values ahead of the model, respectively. An additional Omegadyne® 143PC01D *±1 psid* differential pressure transducer sensed the wall static pressure at the pitot probe location. A 12-bit National Instruments PCMCIA data acquisition card sampled the measured data. Results were logged on a laptop computer running Labview 10®. Figure 9 shows the model mounted in the tunnel. The backside tunnel wall has been removed to allow greater visibility for this picture.

The support rod allowed the model to be positioned at a variety of vertical settings, and at each setting the probe was swept across the wake recording local differential pressure (proportional to airspeed). The linear potentiometer senses the horizontal probe position, and allows a nearly continuous horizontal pressure distribution to be measured. For each complete survey a total of 8 evenly spaced horizontal sweeps were obtained for vertical locations from *60 mm* above to *60 mm* below the center waterline of the model. Complete wake surveys were obtained with the tunnel speed setting at 50%, and 100% power level. Multiple wake surveys were obtained for these tunnel speed settings to allow ensemble set averaging and noise filtering to be performed.

Applying the method developed by Whitmore, Sprague, and Naughton,[7] the drag coefficient can be expressed as a polar area integral of the total momentum defect in the wake

$$C_D = \frac{8}{\pi \cdot D_{body}^2} \int_0^{2\pi} \left[\int_0^{\delta_{wake}} \left(\frac{u}{V}\right)_{r,\varsigma} \cdot \left(1 - \left(\frac{u}{V}\right)_{r,\varsigma}\right) \cdot r \cdot dr \right] \cdot d\varsigma \quad (20)$$

In Eq. (20) the parameter $(u/V)_{r,\zeta}$ is the local normalized velocity defect. The local velocity defect is calculated by interpolating the wake survey velocity defect data at the proper coordinate location (r,ζ) in the flow field.
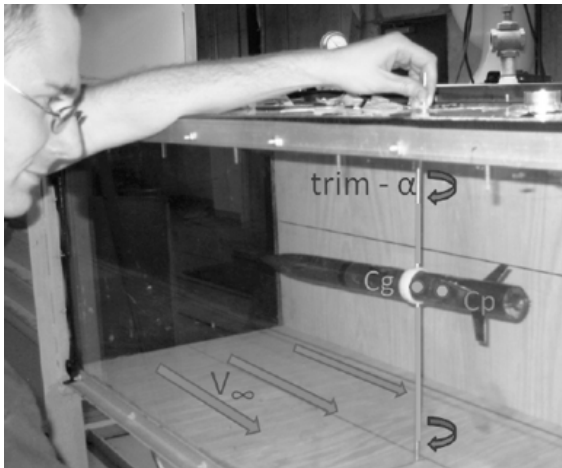
FIGURE 9. 1/5TH SCALE MODEL AND INSTRUMENTATION
LAYOUT FOR WIND TUNNEL TESTS.

The local velocity defect is calculated from the pitot/static pressure data assuming incompressible flow and no tunnel stagnation pressure loss from the reference port to the probe station. The coordinates *(x,y)* represent the local vertical and horizontal position of the probe tip. The probe tip was axially positioned approximately 4 cm behind the model.

Figure 10 shows the filtered and processed results of a typical wake survey. Here the normalized velocity defect *u/V* is plotted as a function of the vertical (*z*), and lateral horizontal (*y*) position behind the model. Axial, top, and isometric views of the wake survey data are presented. Several features are clearly visible including the three model fins and the base wake. The data show very good axial symmetry indicating that a zero angle of attack condition was measured.
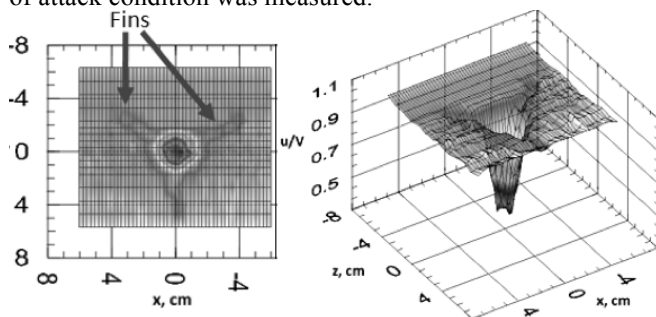
FIGURE 10. TYPICAL WIND TUNNEL SURVEY RESULTS
SHOWING VELOCITY DEFECT IN MODEL WAKE.

Drag Coefficient Comparisons

Figure 11 compares the drag coefficients obtained from the previously described analytical methods and the wind tunnel wake surveys. Here the wake survey C_{D0} has been adjusted for compressibility using the Prandtl-Glauert[8] subsonic correction for comparison with the other models. Not surprisingly the wind tunnel data show the highest drag coefficient. This result is likely due to Reynold's number scaling and surface roughness effects. Based on this ensemble of data, the mean C_{D0} is approximately *0.365* with a standard deviation of *±0.17* (95% confidence level based on 5 ensemble members).
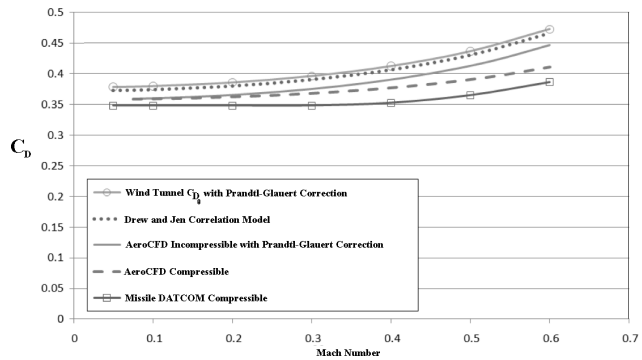

FIGURE 11. DRAG COEFFICIENT COMPARISONS FOR
VARIOUS ANALYTICAL AND EXPERIMENTAL SOURCES.

*VII.2. Main Motor (Cesaroni L-730) Thrust
Measurements.*

As presented earlier in the *Systems Engineering* section, the manufacturer's specifications for the Ceraroni L-730 predict a mean thrust level of *730 N*, a burn time of *3.8 seconds*, and a total impulse of *2765 N-s*. Early flight simulations showed that these motor capabilities achieve the mission objectives. However, because of the well known potential for large motor thrust and total impulse variations, it was imperative for the Chimaera team to procure and test multiple motor reloads to establish the true mean motor parameters and accompanying uncertainties. Test data gathered from three independent motor burns was compared to existing published data for the L-730 motor.

An existing 6-degree of freedom static test at Utah State University was used to perform the motor tests. Only the axial (thrust), and vertical (weight) load measurements were used for these tests. The thermocouples mounted on the external motor case measured the temperature during and after the burn. This temperature measurement was required to insure that the motor case did not exceed operating limits for the flight hardware. Because the USLI rules precluded modifications of the stock motor, chamber pressure was measured for the initial thrust stand shakedown tests, but was not measured for the L-730 characterization tests The chamber pressure measurements required modifying the motor cap with a threaded access port.

The axial load was sensed by an Omegadyne[®] LCCB-500 *2225 N (500 lbf)* load cell. Vertical loads were sensed by two Omegadyne[®] LC101-25 112 N (25 LBF) Load Cells. Both load cell types provided *3mV/Volt* output. Type-K thermocouples were used for the case temperature measurement. Data acquisition was performed using the 16-bit National Instruments Compact-DAQ[®] Universal Serial Bus (USB) data acquisition system. Data were monitored and logged using a test laptop running Labview[®] 10. The test laptop resided within the test cell. A remote laptop, located in the control room, was used to log into the test laptop via Ethernet and a remote desktop application. Remote access was a safety to protect the test team in the event of a motor explosion. Figure 12 shows the thrust-stand instrumentation system and an image of a candidate

rocket motor being tested. The motor was ignited using the normal flight launch.

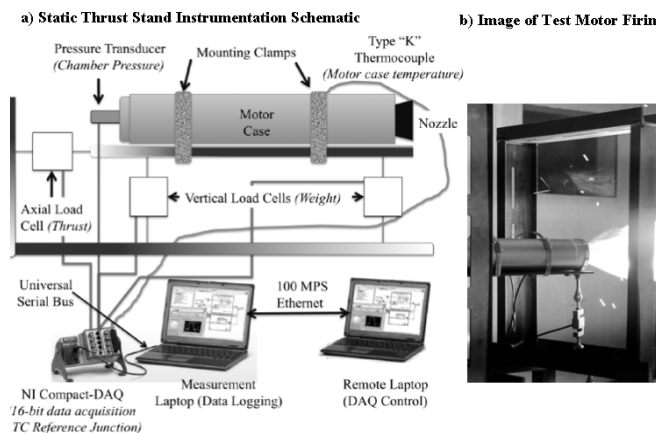a) Static Thrust Stand Instrumentation Schematic   b) Image of Test Motor Firin

FIGURE 12. ROCKET STATIC THRUST TEST STAND.

Figure 13 shows results from the characterization tests where the thrust and impulse burn-time profiles are compared against existing thrust and impulse curves obtained from *Ref. vi* and from the manufacturer.[xiv] All thrust and impulse profiles have been corrected to sea level standard conditions. The thrust profiles show a wide variability in peak thrust and curve shapes; however, the total impulse curves are reasonably consistent. Interestingly, the one motor test that exhibited the lowest peak thrust level, also had the highest overall impulse level. This outlier test was conducted on a particularly cold day (the test cell is open to ambient conditions), and grain temperature is the likely source of this variability.
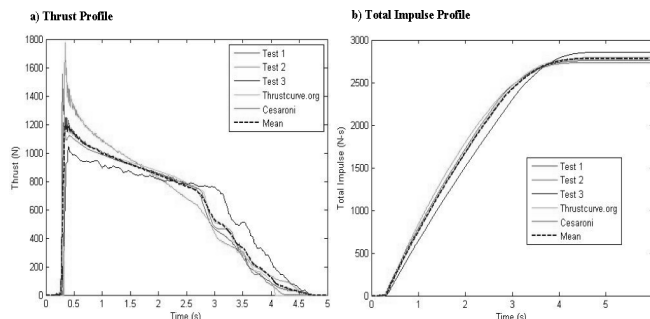

a) Thrust Profile   b) Total Impulse Profile

FIGURE 13. THRUST AND IMPULSE BURN-TIME PROFILES FOR CESARONI L-730 MOTOR.

The mean total impulse is *2779 N-s (624.90 lbf-s),* with a standard deviation of *±47.25 N-s (±10.62 lbf-s).* With 4 degrees of freedom (5 data sets), the 95 percent confidence uncertainty of the total impulse is *±131.28 N-s (±29.51 lbf-s).* The 95% confidence interval variation of total impulse is *±4.7* percent, significantly less than the 20% motor-to-motor variability that was expected. Thus, the L-730 motor reloads were verified as completely acceptable to meet the program requirements.

[xiv] "Cesaroni Pro 54®," http://www.pro54.com, [Retrieved 14 July 2011].

VII.3. C-BAS Characterization Tests

C-BAS characterization ground tests were performed using a custom designed test stand. Figure 14 shows a schematic of the test apparatus, and an image of the thrusters "firing". Axial loads were measured using an Omegadyne® LC101-25 112 N (25 LBF) Load Cell and the regulator output pressure was sensed measured using an Omegadyne® PX139 3450 kPa (500 psia) absolute pressure transducer. A type-K thermocouple was mounted to the regulator outlet to monitor temperature. The C-BAS port side ramp pressures were measured using the flight transducers described earlier in the *Payload Overview* section. A National Instruments NI-6009® 14-bit USB Data acquisition device was used to sample the data. The solenoid valve was controlled using a National Instruments USB-9472 digital relay device. Data were monitored and logged using a test laptop running Labview® 10.
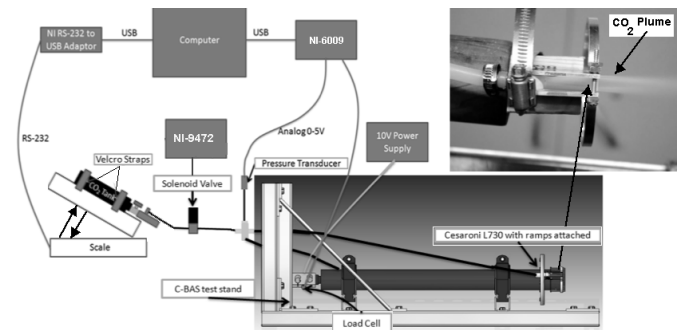

FIGURE 14. C-BAS STATIC THRUST TEST STAND.

Line losses downstream of the regulator outlet were small enough that the sensed pressure was assumed to be identical to the actual aerospike thruster plenum pressure. Rubber support bands were used to constrain the empty test motor with aerospike thrusters attached. These support bands allowed complete transmission of axial forces but constrained lateral movements. The CO_2 tank was elevated at a 45-degree angle to insure that only liquid propellant leaves the tank. The tank weight was monitored during the test using a commercial parcel scale with a serial output.

Figure 15 shows representative test results from a ground test where the solenoid was pulsed in two-second intervals with a 50% duty cycle to emulate the on-off flight operation of the C-BAS. A 20 second duration test was performed to approximate the anticipated time-of-flight to apogee for the vehicle. Figure 15a plots the outlet pressure time history, Figure 15b plots the thrust, and Figs. 15c, d, and e plot the surface ramp pressures. Figure 15f plots the total accumulated impulse.

The measured regulator pressure is not constant for the pressure pulses; but instead peaks sharply, and then decays over the course of the pulse following a first-order decay pattern. This pattern is an artifact of the regulator dynamics, and could not be modified for the current design. A slight drop in the measured outlet pressure for successive pulses can also be seen in these

graphs. The resulting thrust pulses exhibit a similar "peaked" shape. Interestingly, while the outlet pressure remains relatively constant for each of the solenoid pulses, the thrust levels continually drop.

Comparing the predicted thrust levels, which assume adiabatic flow, the thrust drop indicates that the system is getting continually colder as the liquid CO_2 flashes to vapor and expands. As the thrusters cool, the plenum pressure drops and the thrust level drops proportionally. This total impulse comparison also clearly supports the "cooling" hypothesis. The predicted total impulse for the 20-second test is approximately 95.8 N-s, the measured impulse is 75.6 N-s, and represents a loss of approximately 23%. Fortunately, the majority of the impulse loss occurs after 15 seconds of pulsed operation. For flight conditions, after fifteen seconds following main motor burnout the vehicle is near apogee. Thrust and impulse levels required to trim the vehicle are low near apogee.

VIII. Flight Test Results

A total of three Javelin test flights were performed during the 2010-2011 academic year; two qualification flights in preparation for the USLI competition, and the final competition flight. For the team to qualify to participate in the USLI competition, at least one successful launch and recovery prior to the USLI-mandated flight readiness review (FRR) was required The compressed time scale of the USLI competition schedule allow very little time for the flight teams to "wring out" their flight systems through a conservative envelope expansion process. Thus the qualification tests flights often involve an "all or nothing" mentality. As will be described in the next section, this approach very nearly cost the USU Chimaera design-team entry into the USLI competition. The flights were a very humbling learning experience for the entire team. But as former Deputy Administrator of NASA Dr. Hugh Dryden has been famously quoted, "[The purpose of flight research] is to separate the real from the imagined problems and to make known the overlooked and the unexpected."
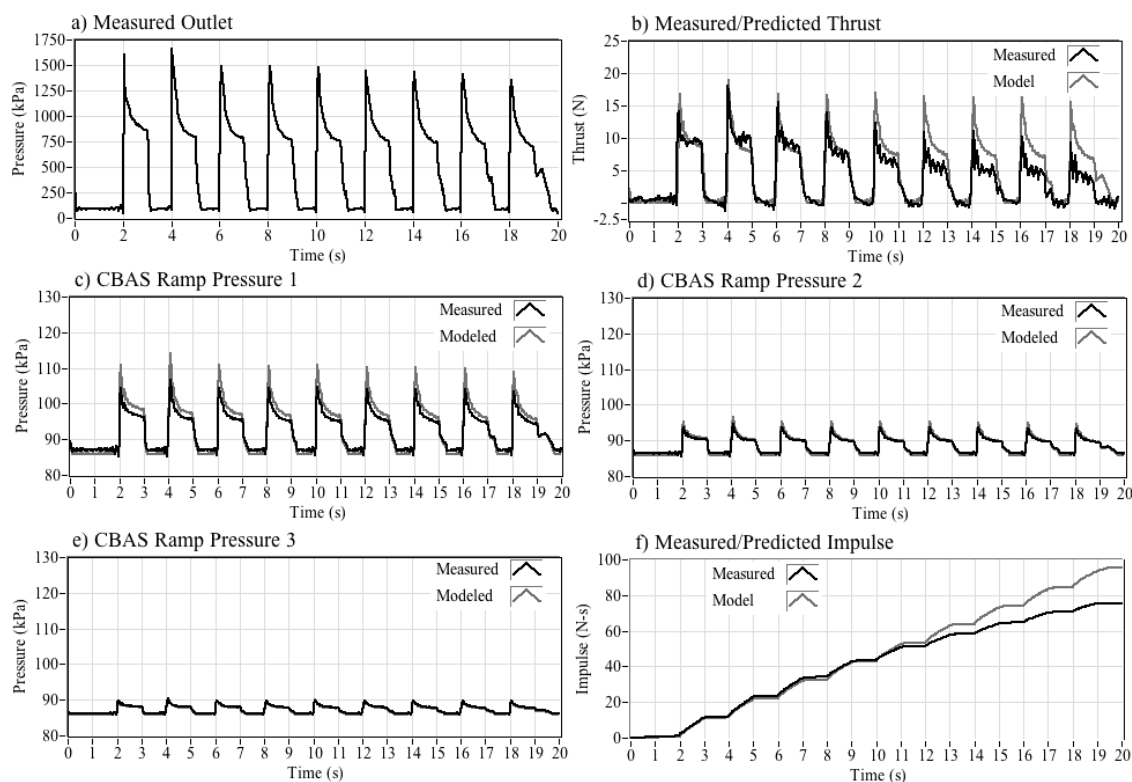

FIGURE 15. REPRESENTATIVE C-BAS GROUND TEST RESULTS.

VIII.1. Preliminary Test Flights.

The first test flight of the Javelin occurred on March 19, 2011 at the Pony Express Test Range outside of Lehi, Utah. Conditions at the site were less than ideal. Sustained winds of *20 kts* and gusts exceeding *30 kts* mph made launch preparations a challenge. The first test flight attempted to fly all of the vehicle subsystems, and had a successful launch but a recovery system failure. The failure resulted in a hard landing

and the vehicle sustained significant damage. Fortunately, many of the vehicle sub systems remained intact including most of the avionics. Unfortunately, the hard impact damaged the IMU and detailed trajectory information was not obtained from that flight. A backup engineering development unit (EDU) was used to replace the damaged unit for the USLI competition fight.

The second flight occurred on March 26, 2011 at the Pony Express test range. The primary objective of this

second flight was to successfully launch and recover the vehicle. Collecting a minimal set of trajectory data to verify the successful flight was an important secondary objective. To simplify operations the vehicle was not fully instrumented with the full avionics suite. Instead only the two PerfectFlite altimeters, the recovery systems components, and power distribution boards were flown. A separate R-DAS system was flown to log the vehicle acceleration and altitude. The IMU, Gumstix flight computer, and telemetry systems were not flown. The C-BAS hardware was flown, but was not activated during flight.

The Javelin was successfully launched and recovered. Salvaging, rebuilding, and flight testing a rocket of this complexity in a single week was a remarkable achievement for the Chimaera team. Again, for this flight the weather conditions were less than ideal with 20-25 knot winds and very cold conditions. For flight 2 the vehicle only achieved an apogee altitude of 1000 meters above ground level.

During pre-launch preparations the launch pad team noted that the vehicle was significantly harder than normal to slide onto the launch rail. Thus, it appears that the blustery conditions blew up considerable sand and silt which partially clogged the slots on the launch rail. During launch the rail lugs partially bound up causing the vehicle to depart at a lower than planned rail velocity. This low launch velocity coupled with the high cross winds caused the vehicle to pitch by approximately 20 degrees as it departed the rail.

Simulation calculations show that the vehicle went through apogee with a horizontal velocity exceeding *70 m/sec*. Much of the potential altitude was wasted as unnecessary horizontal velocity. Fortunately, L-730 motor appeared to have burned nominally, and the simulation comparisons verify that the preflight prediction for drag coefficient is close to what was actually achieved.

Based upon this analysis, and the successful launch and recovery, the Chimaera team felt confident to press forward with the competition launch. Several minor changes were made to the vehicle to gain a higher launch "ΔV." The launch rail was scrubbed, polished, and dry-lubricated to make it significantly "slicker." To prevent binding original plastic launch lugs were replaced with aluminum lugs. The very rough surface coat of the second launch airframe was made significantly less "draggy" by better sealing on the avionics and C-BAS bay access doors, painting and sanding the airframe surface, and applying a plastic MonoKote® film to the airframe.

VIII.2. Competition Flight Test Results.

The 2011 USLI launch competition was held on April 17, 2011 at the Bragg Farms launch site in Toney Alabama. A total of 29 university teams were entered into the competition, but technical difficulties kept several of the teams from actually launching. According to the competition PerfectFlite altimeter, the Javelin achieved an altitude of 1665 meters (5465 ft) above the launch ground level. Of all the teams entered into the USLI competition, this altitude was the 7th closest overall The competition altimeter varied slightly from the back-up recovery system altimeter, which read 1659 meters (5443 ft). The discrepancy shows the lack of fidelity in low-end hobby rocketry components.

There are several factors that could have produced the higher than anticipated apogee altitude (3.5% error). Clearly, a less than vertical initial launch angle would produce a lowered apogee and is not a possible cause. The Chimaera team identified 5 most likely causes for the higher apogee; these are 1) lower than expected vehicle launch weight, 2) in-flight thermals and updrafts, 3) an anomalously large C-BAS total impulse, 4) an anomalously large L-370 motor burn impulse, and 5) lower than expected in-fight vehicle drag. Comparing the measured pre-and post launch weights with the expected values quickly eliminated items 1 and 3 in this list. The recorded pre flight weights agreed with the expected weight by less than 10 grams. Also, the post flight CO_2 tank weight indicated that no propellant was consumed; the C-BAS system did not operate. Similarly, Item 2 in the list was also quickly eliminated. The launch day was cool and stable with clear skies. A check of local national weather service records indicated a building area of high-pressure into the region. This synoptic pattern makes substantial thermal activity very unlikely. Thus by the process of elimination, only the anomalously high L-730 burn impulse, and reduced drag hypotheses remained as likely explanations. These two factors will be investigated in the following subsections.

Cesaroni L-730 Motor Flight Burn Profile

Figure 16 compares longitudinal acceleration during the climb to apogee and accumulated "ΔV" in *g-s* (the integral of the longitudinal acceleration) as measured by the IMU against simulation calculations perform using the best estimates of vehicle launch mass (*12.59 kg*) and drag coefficient ($C_{D0} = 0.365$). Since the post flight inspections verified that the C-BAS did not operate in flight, the simulation calculations assume no energy augmentation. Clearly, of flight while the motor is burning during the initial stages the acceleration and ΔV traces are nearly identical. Clearly, there is nothing anomalous about the burn profile of the L-730 motor. However, just before motor burnout, the flight data shows a slightly greater acceleration level, and the ΔV curves begin to diverge.

When the simulation is re-run, but with a 25% lower drag coefficient ($C_{D0} = 0.285$), the flight and simulation time history traces are nearly identical. Figure 17 shows this comparison. These comparisons support the conclusion that the vehicle clearly experienced a lower drag-level in the competition flight than was predicted by the analytical models, wind tunnel tests, and the
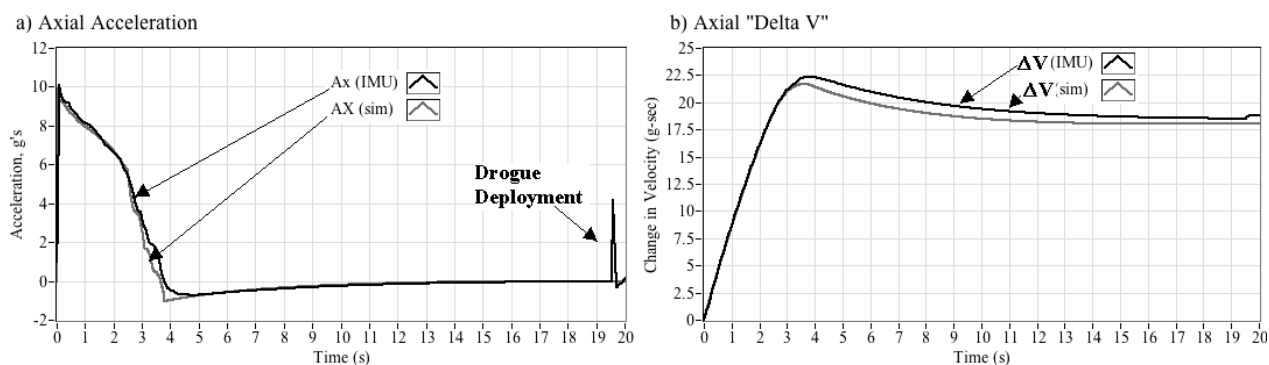
flight 2 trajectory data.

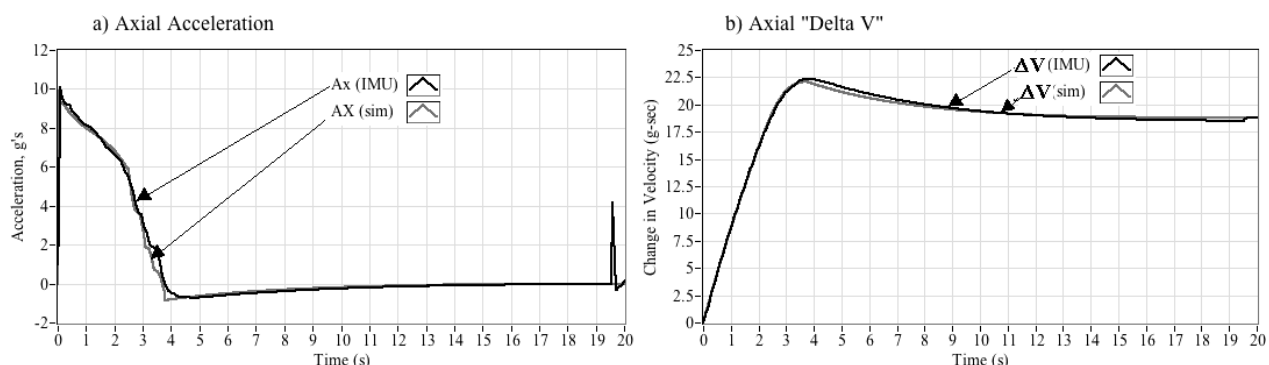FIGURE 16. COMPETITION FLIGHT AXIAL ACCELERATION AND ΔV COMPARED TO SIMULATION WITH $C_{D0} = 0.365$.

FIGURE 17. COMPETITION FLIGHT AXIAL ACCELERATION AND ΔV COMPARED TO SIMULATION WITH $C_{D0} = 0.285$.

Effect of Lowered Drag Coefficient

Figure 18 presents additional data to support this "reduced drag" hypothesis. The first graph 21(a) compares the altitudes and potential altitudes calculated from the competition Perfectflite altimeter and the IMU/Kalman filter with the simulation results assuming $C_{D0} = 0.365$. The second graph 21(b) repeats the comparison with $C_{D0} = 0.285$. In the first graph, the simulation predicts an apogee altitude of 1546.91 meters. In the second graph the simulation predicts an apogee altitude of 1663.03 meters, a value almost identical to the measured Kalman filter apogee, 1664.1 meters. No energy augmentation is active for any of the time history traces. Figure 18b also plots the target altitude schedule for C-BAS activation.

Because of the reduced drag, it is very likely that the energy bleed off during the ballistic phase of flight was lower than anticipated, and the overall energy level never crossed over the scheduled value for triggering C-BAS activation. Figure 18b compares the measured altitude, predicted altitude, and potential altitude against the C-BAS target altitude schedule. Following the main motor burnout at 3.8 seconds, the target schedule always remains below the calculated potential altitude trace. As a result, the C-BAS activation algorithm "energy-low" event was never detected, and the energy management system was never operated.

Plausible Reasons for Reduced Drag Coefficient on the Competition Flight.

Reasons for the drag reduction from flight 2 to flight 3 are unclear; however, a significant reduction in skin friction is a likely cause. For the qualifying flight the vehicle was unfinished, and the airframe had a relatively rough sanded epoxy surface with gaps for the access doors. This rough surface likely tripped the flow and resulted in forced bypass turbulence very far forward along the body contour. Three changes implemented for the competition flight may have reduced this bypass transition effect. In preparation for the competition flight the Javelin was covered in hi-gloss MonoKote® over the majority of the exposed surface area, and a high-gloss paint was applied to the nosecone.

Additionally 3.5 cm of length were removed from the center of the rocket to adjust the center of gravity. This reduction in the length of the rocket gave a lower Reynold's number and lessened the surface area that was exposed to turbulent flow. Finally, tape was added to secure the access doors. Rather than the gaps that were present on the flight 2 configuration; the tape created a continuous surface further removing turbulent triggers from the rocket. These three feature changes may have allowed a significant extension of laminar flow on the body. Extended laminar flow, if it occurred, would have produced a significant overall
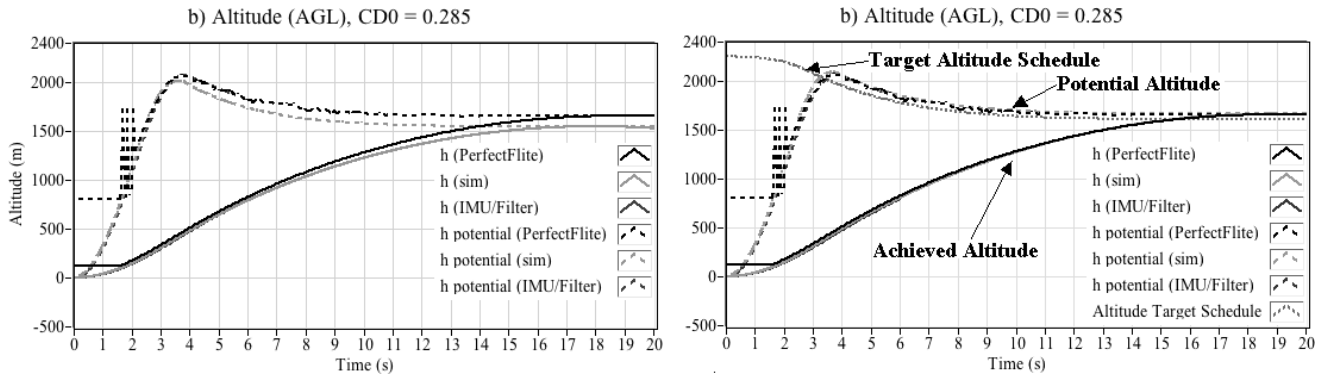
drag reduction.

FIGURE 18. ALTITUDE AND POTENTIAL ALTITUDE COMPARISONS FOR NOMINAL AND REDUCED DRAG PROFILES.

First-Order CFD Solutions

To investigate this premise, a computational fluid dynamics (CFD) analysis was performed to examine the effects laminar and turbulent drag on the Javelin. A control volume and computational mesh was created and solved using the commercially available CFD code Fluent[xv]. Tetrahedral elements were used at an interval size of 100 units in the control volume. The boundary condition for the upper surface of the control volume was prescribed as a solid boundary to further speed convergence time. The Fluent[®] model has 523,980 cells, 1,092,745 faces, and 110,424 nodes.

To benchmark the highest overall drag value, highest velocity during flight, 185 m/sec (Mach 0.5) was chosen as the inlet condition. This peak velocity occurred at 640 meters above sea level. A laminar model and three different turbulence models were used to calculate the drag coefficient. The model was solved assuming and incompressible fluid using the SIMPLE scheme with first-order up-winding. In the interest of time, higher order solutions were not attempted. Table 7 summarizes the results.

Not unexpectedly, the drag coefficient values presented in Table 5 are low when compared to the baseline calculations for the Javelin. Possible reasons for this difference include induced drag due to fin misalignment vehicle spin, local angle of attack variations during flight, and an improperly modeled vehicle base area. Taking these factors into account, the difference between the average incompressible turbulent drag coefficient of *0.2790* and the incompressible laminar drag coefficient (*0.2046*) is 0.*074*. This value comparable to the drag coefficient reduction observed in the flight data of *0.080*, and lends credence to the re-laminarization hypothesis. Ultimately, the reason for the dramatic decrease in drag from *flight 2* to the *flight 3* can only be discovered with significantly more experimentation and flight-testing.

TABLE 5. CFD PREDICTED JAVELIN DRAG COEFFICIENT FOR VARIOUS VISCOSITY/TURBULENCE MODELS.

Model	Drag Coefficient
Laminar	0.20464
Spalart-Allmaras	0.27690
k-epsilon	0.25172
k-omega	0.3084

Aerospike Ramp Pressures

Even though the C-BAS did not activate in-flight, pressure data were still successfully logged, and provided useful modeling information. This data can be used to infer the in-flight performance of the C-BAS had it actually operated. Figure 19 shows sensed differential pressure normalized by dynamic pressure to calculate corresponding pressure coefficients, plotted as a function of free stream Mach number. The pressure coefficients on the ramps show very negligible effects due to Mach number – as least for the moderate subsonic pressures experienced in flight. Wang et al,[9] have observed that Mach number has a significant influence on cross-flow effects only under supersonic conditions -- so this result is not entirely unexpected.

When the mean pressure coefficients calculated from the C-BAS ground tests of Figure 15 are combined with the flight slipstream pressure coefficients, an in-flight linear subsonic performance model for the C-BAS thrusters is created. Figure 20 shows this result. Here the flight pressure coefficients, demonstrated to be independent of Mach number, are plotted as a function of the longitudinal distance down the spike ramp. The three pressure port coefficients have been curve fit to give a continuous distribution along the ramp surface. Similarly, the C-BAS ramp ground pressure coefficients, calculated as the surface ramp differential pressure divided by the plenum pressure are plotted as function of the longitudinal distance down the ramp. These pressure coefficients are multiplied by a factor of 10 to give a similar display magnitude as the flight pressure coefficient

---

[xv] "Flow Modeling Solutions for the Aerospace & Defense Industries," Fluent, Inc., http://www.fluent.com/solutions/aerospace/index.htm [Retrieved: 14 July 2007].

data. The predicted in flight thrust levels can be calculated by integrating the pressure forces displaced on this figure along the length of the ramp, summing the two results, and adding the momentum thrust at the throat exit.
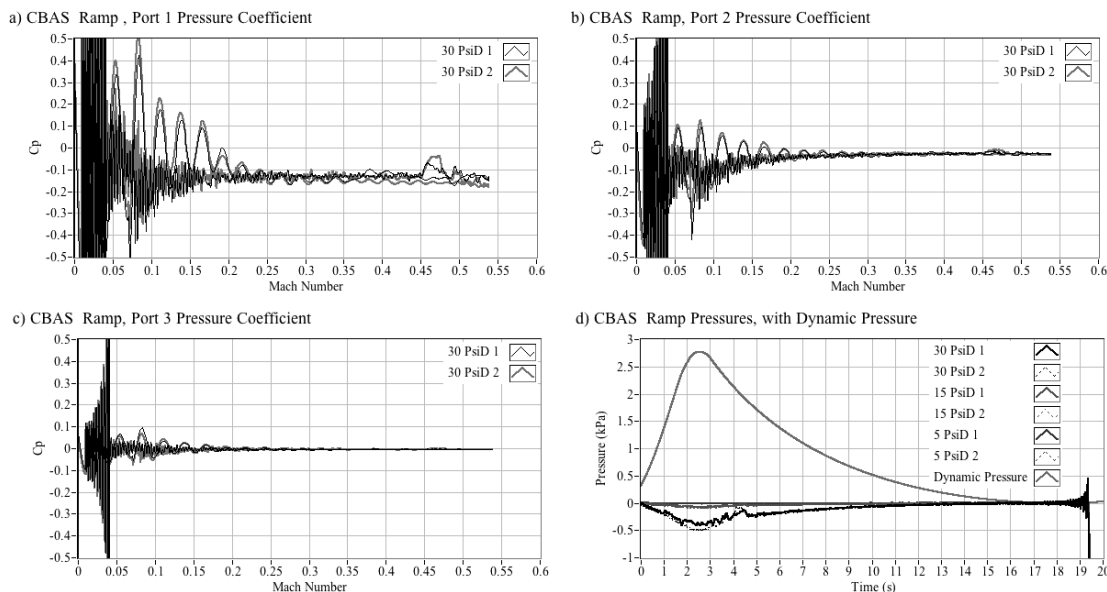

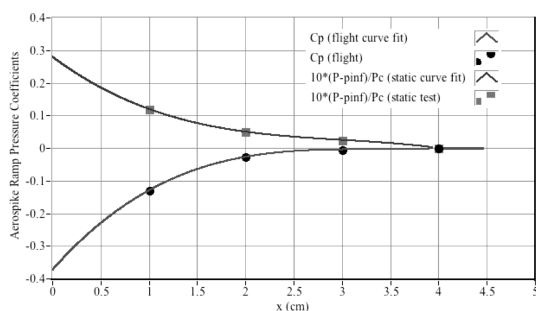FIGURE 19. AEROSPIKE RAMP IN-FLIGHT PRESSURE COEFFICIENT MACH NUMBER PROFILE.

FIGURE 20. IN-FLIGHT LINEAR C-BAS THRUSTER
PERFORMANCE MODEL.

IX. Summary and Conclusion

This paper describes the development and implementation of an advanced capstone senior design course at Utah State University, Logan Utah. This paper is offered as a case study of a successful course, and it is hoped that the presented materials will serve as a guide for other academic institutions wishing to under take a similarly ambitious project. Ultimately, the Utah State Chimaera team was selected as the winner of the 2011 NASA launch competition.

In industry, the client or customer provides much of the program structure including design requirements, budget, and program schedule. These constraints do not exist in an academic design class. Here, typically the instructor must artificially prescribe the budget, design requirements, and schedule. One of the positive aspects of building an academic course around an externally sponsored competition is the clearly defined, realistic set of requirements that are set by the competition rules.

The design features a solid-propellant primary rocket motor that provides a majority of launch impulse, and a secondary cold-gas propulsion system that manages the energy level of the vehicle to reach a target apogee altitude. The secondary propulsion system was flown as the "engineering payload" for the USLI competition. The secondary system features a pulse-modulated cold gas bleed system with expansion ramps designed from aerospike nozzle theory. The energy management system was integrated with the airframe by placing the aerospike ramps around the primary solid motor case; this design added minimal aerodynamic drag to the configuration. Onboard navigation data are processed in a small avionics computer to continuously estimate the total specific energy and potential altitude of the vehicle. When, required, the onboard avionics activate the system and boost the energy level of the vehicle.

With all factors considered, The Javelin launch at the USLI competition was a success. With a flawless launch and parachute deployment, the only flight anomaly was an anomalously low drag coefficient when compared to qualification flight data and pre-flight predictions. Because of the reduced drag, energy bleed off during the ballistic phase of flight was lower than anticipated, and the overall energy level never crossed over the scheduled value for triggering C-BAS activation. Flight IMU data relayed wirelessly during flight clearly shows that the rocket had an otherwise nominal flight trajectory. While the C-BAS did not activate, in-flight pressure data was still successfully logged, and provided useful data. This data can be used to infer the in-flight performance of the C-BAS had it actually been operated.

Throughout the one-year process of designing, reviewing, fabricating, and flying, the students learned that no "correct answer" existed; only extensive analysis, redesign, and verification testing produces a successful prototype. This experience is not conventionally provided by academic coursework. The lessons learned from failure are equally as important as those learned by success. When the original rocket was lost in the crash, no finger pointing fingers and laying of blame occurred; instead the team as a whole responded as champions. Salvaging, rebuilding, and flight-testing a rocket of this complexity in a single week was a remarkable achievement. Recovering from the disaster to win the overall USLI competition title was real demonstration of student character. Involvement in the accident investigation board, provided the team with the opportunity to learn from errors made, and will go a long way to making them better design engineers.

For the 2011-2011 academic year, the USU Chimaera Team has been invited to participate in NASA's advanced university flight demonstration program at Wallops Flight facility, Virginia. An evolved version of the C-BAS system will be retained as the primary payload. It is hoped that several successful in-flight demonstrations of the C-BAS system will occur during this time period.

Acknowledgements

Authors' information

[1]Associate Professor, Utah State University Mechanical & Aerospace Engineering Department, 4130 Old Main Hill/UMC 4130. Logan UT 84322-4130, USA.

[2]Graduate Research Assistant, USU MAE Department, Logan UT, USA.

Stephen A. Whitmore was born in Nelsonville, Ohio, USA, on November 19, 1956. Dr. Whitmore attended undergraduate school at the University of Illinois, Urbana IL, where he graduated with a BS in Aerospace Engineering (1979). He attended graduate school at the University of California, Los Angeles CA, where he received MS, engineer, and doctoral degrees in Aerospace Engineering.

Dr. Whitmore is an associate professor of mechanical and aerospace engineering at Utah State University. He joined USU in 2005 after years working for the National Aeronautics and Space Administration for more than 25 years. Dr. Whitmore is an Associate Fellow of the American Institute of Aeronautics and Astronautics (AIAA), has is currently a member of the AIAA Space Systems and Hybrid Propulsion Technical Committees.

Dr. Whitmore has published over 100 technical monographs including NASA technical memoranda and technical reports, conference papers, book chapters and peer-reviewed journal publications. He has 4 patents and has received multiple national awards including the NASA Engineering Achievement Medal and Utah Engineering Educator of the Year.

Dr. Whitmore is director of the Chimaera Hybrid Rocketry program at USU. The USU senior design teams lead by Dr. Whitmore have won the NASA-sponsored University Student Launch Initiative (USLI) Competition at Huntsville Alabama three times including the 2007-2008, 2008-2009, and 2010-2011 academic years.

References

[1]   Lee, Ching-Che, and Thompson, D. D., "Fortran Program for Plug Nozzle Design," NASA TM X-53019, Washington DC, July, 1964.

[2] Miyamoto, H., and Matsuo, A., and Kojuma, T., 42nd "Effects of Sidewall Configurations on Rectangular Plug Nozzle Performance," AIAA 2006-4373, *43rd AIAA Joint Propulsion Conference and Exhibit, Sacramento, CA, 9-12 July, 2006.*

[3] Etkin, B., *Dynamics of Atmospheric Flight*, John Wiley and Sons, New York, 1972, Chapt. 5.

[4] Blake, William B., "Missile DATCOM User's Manual - 1997 Fortran 90 Revision", Air Force Research Laboratory, February 1998.

[5] Drew, B, and Jen, A., "Pressure Drag Calculations on Axisymmetric Bodies of Arbitrary Moldline", AIAA-90-0280, *28th Aerospace Sciences Meeting and Exhibit, January 8-11, 1990, Reno, NV.*

[6] Barrowman, J.S., "The Practical Calculation of the Aerodynamic Characteristics of Slender Finned Vehicles", Catholic University of America MS Thesis, March 1967.

[7] Whitmore, S. A., Naughton, J. W., and Sprague, S., "Wind-Tunnel Investigations of Blunt-Body Drag Reduction using Forebody Surface Roughness," AIAA-2001-0252, January 2001, *39th Aerospace Sciences Meeting and Exhibit, January 8-11, 2001, Reno, NV.*

[8] Kuethe, A., M., Chow, C., Y., *D*, 3rd ed, John Wiley & Sons, New York, 1976, pp. 258-262.

[9] Wang, C. H., Lui, Y., and Qin, L., Z., "Aerospike Nozzle Contour Design and Its Performance Validation," Acta Astronautica, Vol. 64, No. 11-12, June-July 2009, pp. 1264-1275.